UTRECHT UNIVERSITY

ENERGY IN THE BUILT ENVIRONMENT (GEO4-2522) 2021/2022

Computer practical assignment: Utrecht smart district

Part A: Building-integrated photovoltaics (BIPV) - Irradiance and PV performance modelling

Students:

Kevan Skorna (1540602)
Ruben van Eldik (6976050)
Erik van Battum (5715563)
Rajesh Kumar (0974722)
Marita Hoekstra (5972590)

Course coordinator:

Dr. ir. Ioannis Lampropoulos

Word count:

3088

Tuesday 12th October, 2021

Contents

List of Figures

List of Tables

1 Determine the best model to compute the DNI

This chapter aims to find the best irradiance model for the Netherlands, which will be used to answer the other questions in this report.

1.1 Question 1.1

In the first step of the exercise four different irradiance models (DISC, DIRINT, DIRINDEX, ERBS) are used to compute the direct normal irradiance (DNI) on the pre-determined building site in Utrecht, NL. In a second step, to find the best fitting model for further processing, each model's DNI modelling performance is evaluated by calculating error residuals using a real-word dataset called UPOT and generated in 2015, which contains actual DNI measurements at the specific location in Utrecht, NL.

To prepare the UPOT dataset for this performance comparison only minimal data preparation steps are undertaken. Without any modification to the UPOT dataset, the DIRINDEX model returns infinite values for solar positions below 4 degrees above the horizon. To eliminate that error, corresponding data entries below this threshold are removed from the UPOT 2015 dataset. Since the yearly GHI for solar positions below 4 degrees accounts for only 0.45% of the total yearly GHI, removing these entries will not affect the total results significantly. The time intervals of data entries of the UPOT dataset vary within the time series. While this might result in issues for some data processing applications, the choice was made *not* to resample the data. As mentioned prior, the intended use of this dataset is the calculation of error residuals between the real-world data from the UPOT dataset and the respective irradiance models. For this use-case inconsistent time intervals are irrelevant. On the contrary, data resampling would result in less accurate error function results, as artificial, resampled data entries have a distorting effect.

1.2 Question 1.2

While all error functions contain some useful information, they are not equally appropriate to evaluate model accuracy in this application case. For assessing their applicability towards that end, the *type* of data needs to be considered, which the models aim to replicate.

The type of data, used in this exercise, fall into the category of so-called time series data. One important characteristic of time-series data is that past computed or measured data predicts to a certain degree future data (a value in t-1 has some predictive power for a value in t of the same dataset). This phenomenon is called *auto-correlation* and violates the condition of statistical independence for some error metrics. This is a potential issue. In addition, the measured data from the UPOT 2015 dataset exhibits *seasonality*. These are time-dependent trends within the sample, following relative increases or decreases of monthly average direct normal irradiance (see Figure 1).

Seasonality and auto-correlation particularly inflate the coefficient of determination (RSQR). This reduces its explanatory power, rendering it unsuitable for measuring forecast model accuracy. The same can be said about the MBE. While it provides useful information on systematic model biases, the equation cancels out negative and positive error residuals. Based on this metric, models with large residuals potentially perform similarly well as compared to those with small error residuals. This renders the MBE equally unfit as a reliable measure for model accuracy. Nonetheless, it is noteworthy that the DIRINDEX and ERBS irradiance models appear to be considerably less biased than the DISC and DIRINT models (MBE of 2.41 and -2.25 respectively as compared to -27.3 and -19.2).

The MAE indicates the mean absolute error of a model. That is to say, it takes the arithmetic average of all error terms of the models, regardless of their positive or negative deviance from the measured DNI data. As it's value is expressed on the same scale as the

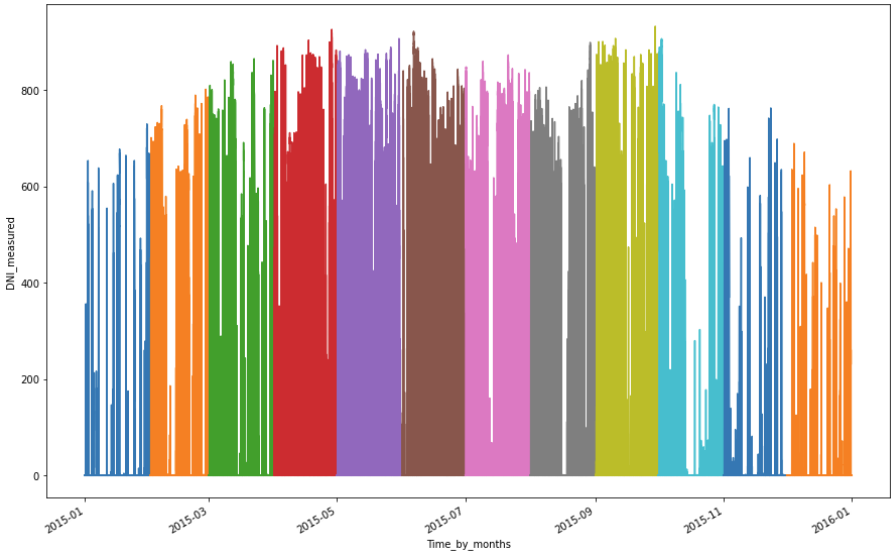

Figure 1: Seasonal variance in UPOT 2015 data

underlying datasets, it is an easy to understand metric. For all models the MAE lies roughly between 52 and 66, with values of the underlying datasets ranging from approximately 0 to 1000. Based on this metric, all irradiance models perform similarly well, complicating a selection of the best model, purely based on this metric. However, taking a closer look at the distribution of error residuals, we can identify that all models have significant numbers of outliers (see Figure 2).

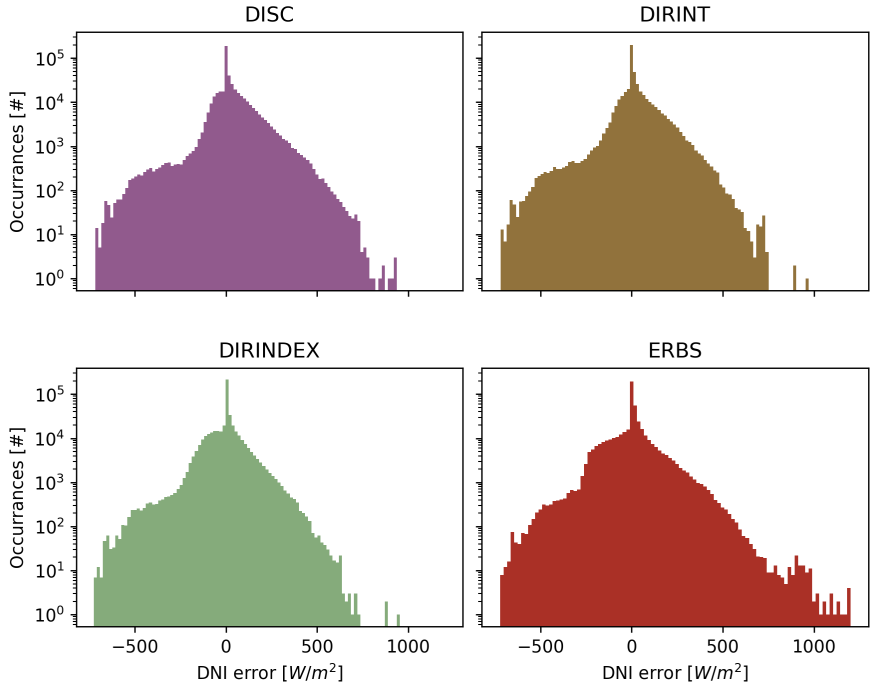

Figure 2: Error distribution of irradiance models on a log scale

Considering that an accurate forecast model should perform well for providing reliable information in small observation intervals (i.e. DNI forecast for selected hours or days of the year) it should not exhibit large numbers of outliers, as they would decrease the reliability

of such forecasts. Consequently an error function, such as the RMSE, which penalises large errors through its exponential equation component, might be the most suitable error function or model selection criterium for this application case, since the model with the lowest RMSE value is likely to have the lowest number of outliers.

1.3 Question 1.3

Table 1: Error function output for each irradiance model

Model	RMSE	MBE	MAE	R^2
DISC	107.56	27.31	59.15	0.891
DIRINT	100.0	19.2	53.45	0.902
DIRINDEX	**94.89**	**-2.41**	**52.89**	**0.898**
ERBS	115.28	2.25	65.63	0.857

Based on the RMSE values and also considering the MAE and MBE output, as supplementary criteria for model accuracy, the DIRINDEX model appears to perform best (see Table 1).

Figure 3[1] visualises the deviance of model outputs from real-world data, with x-values representing measured DNI and y-values computed DNI. The closer the points are towards the regression line, the more the model fits the measured data. The DIRINDEX model shows the best fit with the regression line, which visually confirms the best model fit that the RMSE and MAE error functions indicate.

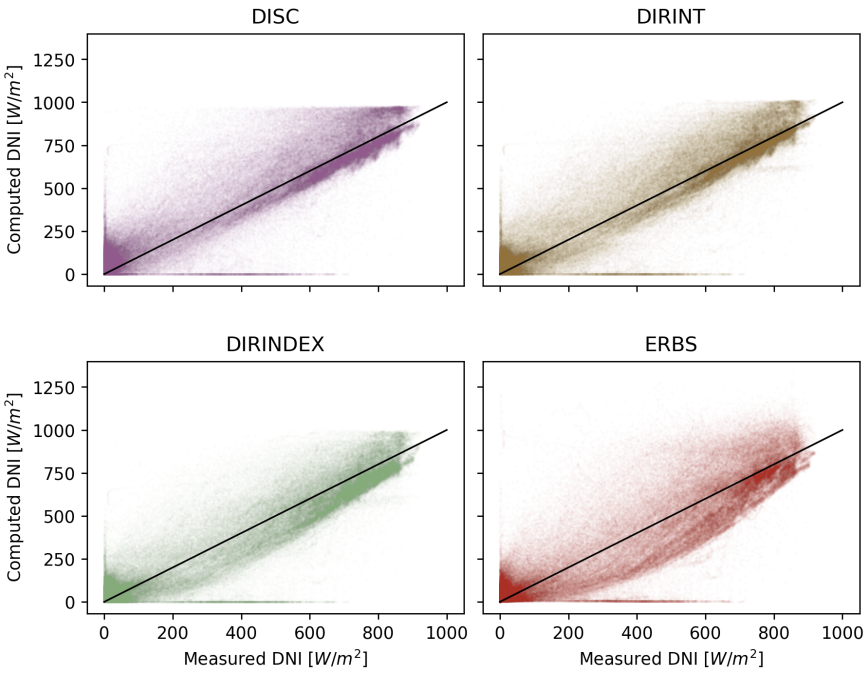

Figure 3: Scatter plot of the measured DNI compared to the calculated DNI

[1]Colors were chosen in accordance with the Japanese philosophy of aesthetics Wabi-sabi. *Source*: Wada, 2011.

2 Determining the plane of array (POA)

Section 2 answers two questions. In doing so, the necessary data is firstly imported and pre-processed, as described in section 2.1 and 2.2. In section 2.4 the optimal position of the rooftop PV systems on building A and B is determined. Finally, the annual irradiance for each surface is calculated in section 2.5 and 2.6.

2.1 Question 2.1

Calculations in this part of the assignment are based on hourly data from the KNMI (Koninklijk Nederlands Meteorologisch Instituut, Royal Dutch Meteorological Institute) weather station in Leeuwarden, the Netherlands (KNMI, 2019). The dataset is prepared for further calculations in the following manner:

1. The data is converted to appropriate units to facilitate calculations - such as J/cm^2 to kW/m^2, and unit values of wind speed and temperature are converted to m/s and degrees Celsius respectively.

2. Date and time columns are merged into one datetime index and localised, applying the UTC time convention to reflect local time.

3. The KNMI data points are extracted on an hourly basis. Data entries are the average values measured within the time span of an hour. The only value that is not averaged is the timestamp, which is set to the start of the hour. This leads to a misalignment between the timestamp and their corresponding data entries. The induced 30 minute discrepancy is removed by shifting timestamps to the middle value of each time interval. Assuming a linear change of measured values over time, this precaution ensures that the recorded average values correspond to the timestamp, in which the specific recorded values would have likely been measured (*e.g.* instead of the first timestamp being at 00:00, the first timestamp is at 00:30, etc).

2.2 Question 2.2

In preparation for the overview Table 2 (see question 2.5 of the report), the surfaces, tilt and orientation of all buildings are described as follows:

1. *Surfaces:* surfaces are expressed in terms of surface type (facade or roof) + the general wind direction that the surface is facing.

2. *Tilt:* tilts are expressed in degrees. The surface is tilted away from the horizontal plane (*e.g.* a vertical facade is expressed as 90 degrees).

3. *Orientation:* The orientation of a surface is expressed clockwise, in degrees. Its perpendicular line is facing away from North (*e.g.* an East facing facade has an orientation of 90 degrees, a West facing facade an orientation of 270 degrees).

Additionally, it is assumed that building A is offset of the grid by exactly 45 degrees, as this is visually suggested in the assignment description. The results discussed above are summarised in Table 2.

2.3 Question 2.3

The POA_{total}, $POA_{diffuse}$, and POA_{direct} are calculated for each of the surfaces on an hourly basis and by using geographic coordinates of the KNMI station in Leeuwarden (NL) as model

inputs. To calculate the yearly POA (in kWh per m^2 per year) from the POA as power (in W per m^2) the power values are first summed and then divided by 1000 which inherently gives annual values in kWh per m^2. For results see Table 2.

2.4 Question 2.4

a. The important step to determine the PV performance, is to find out the total irrandiance on the PV panels's plane of array(POA). The total irradiance (POA_{total}) is comprised of direct (POA_{direct}) and diffused irradiance ($POA_{diffuse}$), which varies due to different tilt and orientation the PV panels. So, to calculate the best tilt and orientation of the solar PV on the non-obvious surfaces (*i.e.* rooftops of building A and B), the same formula is used as for question 2.3 using different tilt and orientation values. The combination of tilt and orientation, which yield the highest total irradiance is determined in the sections below.

b. Figure 4 presents the total irradiance per year, assuming tilt angles from 10 to 40 degrees in 5 degree increments. While the calculated total irradiance does not change by orders of magnitude for each tilt angle, the graph indicates that tilt angles between 30 to 40 degrees perform better.

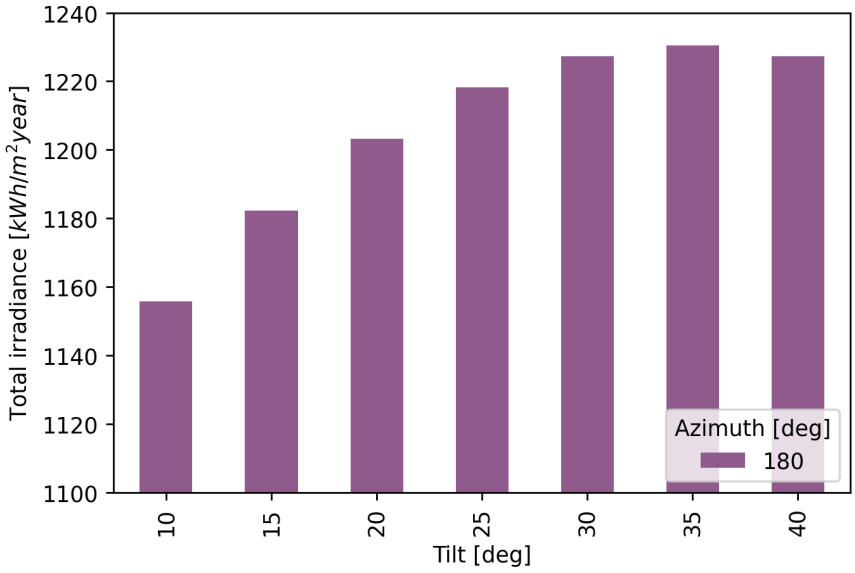

Figure 4: Total yearly irradiance for each tilt for rooftop B

c. Figure 5 presents the total irradiance per year, assuming tilt angles from 10 to 40 degrees in 5 degree increments, for each of the two different azimuths (135 and 225 degrees).

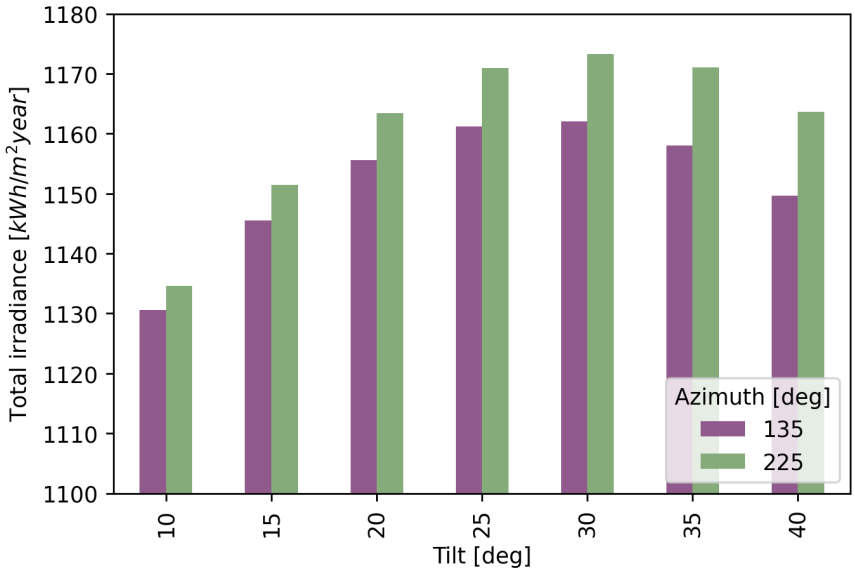

Figure 5: Total yearly irradiance for each tilt and azimuth for rooftop A

d. For rooftop B, with a fixed orientation or azimuth of 180 degrees, the optimal tilt is determined to be 35 degrees, since this appears to receive the highest irradiance, which will arguably result in the highest expected power output of the chosen PV system (see Figure 4). For rooftop A the optimal POA position is determined to be an azimuth of 225 degrees and a tilt of 30 degrees (see Figure 5).

2.5 Question 2.5

After finding the tilt and orientation of certain roofs and facades, finding the optimal tilt and orientation for PV panels on the remaining rooftops and then calculating POA values for each of these surfaces, it becomes possible to compile a table summarising this information. Table 2 shows the tilt and orientation of each surface and the yearly specific $\text{POA}_{\text{total}}$, $\text{POA}_{\text{direct}}$, and $\text{POA}_{\text{diffuse}}$.

Table 2: Overview table displaying all surface orientation and POA values.

Building surface orientations and POA values						
Building	**Surface**	**Tilt [deg]**	**Orientation [deg]**	**$\text{POA}_{\text{total}}$ [kWh/m² yr.]**	**$\text{POA}_{\text{diffuse}}$ [kWh/m² yr.]**	**$\text{POA}_{\text{direct}}$ [kWh/m² yr.]**
A	Facade SW	90	225	832.86	418.50	414.36
	Facade SE	90	135	848.40.	418.50.	429.91
	Roof	30	225	1173.32	545.77	627.54
B	Facade W	90	270	693.47	418.50	274.97
	Facade S	90	180	894.19	418.50	475.69
	Facade E	90	90	677.04	418.50	258.54
	Roof	35	180	1230.38	538.89	691.50
C	Roof S	40	180	1227.24	531.08	696.16
D	Roof W	40	270	990.37	531.08	459.29
	Roof E	40	90	973.12	531.08	442.04

2.6 Question 2.6

Having determined the optimal position of the solar panels on roof A and B, Figure 6 presents an overview of the total irradiance. Table 2 also reveals that solar panels on roofs, facing approximately South (S) receive the highest total annual irradiance (1200kWh per m^2 year). These are the roofs of building A (SW orientation), B (S) and C (S). East (E) and West (W) roofs and facades, facing South-East (SE) as well as South-West (SW), receive significantly less irradiance throughout the year, but still above 800kWh per m^2 year. E and W facades receive the lowest total annual irradiance, with values between 670 and 700kWh per m^2 year. For both facade and roof installations, E and W orientations appear to perform worst.

These results underline the relationship between orientation and tilt and their combined effect on irradiance. While there is not a big impact of orientation on the irradiance received on vertically tilted surfaces, the orientation on tilted surfaces, with a shallow angle (*i.e.* rooftops), is quite noticeable. This might be due to the higher share of diffused light hitting facades, which is less sensitive to orientation changes as compared to rooftops that receive a higher share of direct sunlight, rendering their received total irradiance more sensitive to orientation.

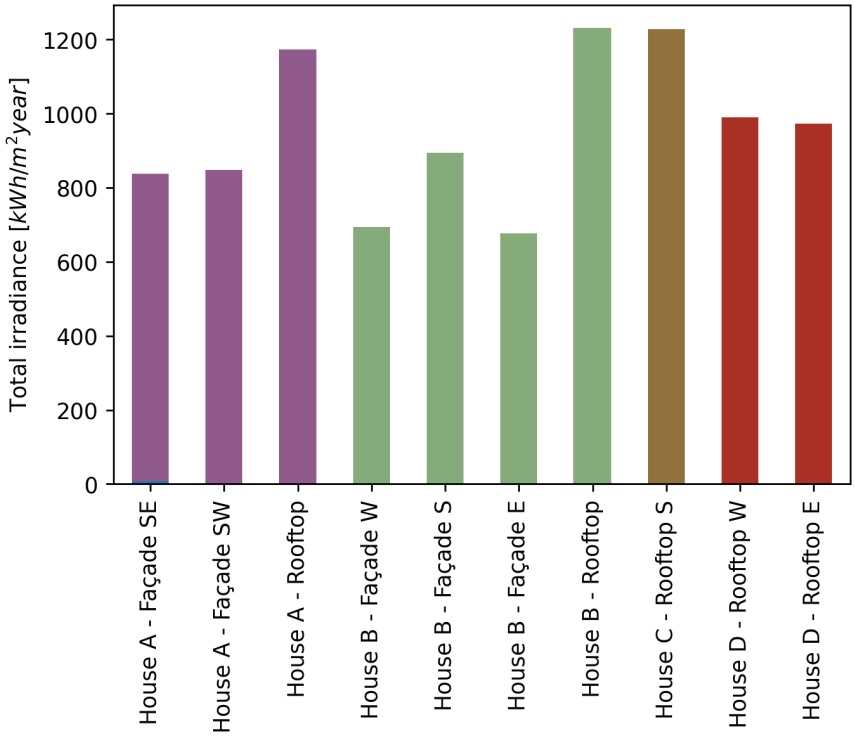

Figure 6: Total yearly irradiance for each each surface

3 Calculating the DC power output

In section 3.1 the number of solar panels, capacity per module type, and rooftop are calculated. This is used to find the performance and annual DC yield, presented in section 3.2 and 3.3. Finally, section 3.4 determines the best module per surface.

With the irradiance and the optimal tilt and orientation of each PV system determined, it is essential to note that PV power generation is dependent on three more parameters:

1. *PV system:* The performance of each PV system is characterized through the inherent material composition of the PV technology. The technologies, studied in this report, are the Sanyo HIT module (heterojunction with thin layer (HIT) hybrid silicon systems), the Yingli mono c-Si module (monocrystaline silicon system), and the FirstSolar CdTe thin-film module (which contain cadmium (Cd) telluride (Te) as their composite elements). The performance of different systems can change during their life cycle (Kunaifi et al., 2020). Hence the time-series monitoring data is used to get further efficiency related information.

2. *PV cell temperature:* PV cells are a type of semiconductor. Semiconductors are sensitive to temperature, as a result the efficiency of a PV module reduces with an increase in temperature (Vidyanandan, 2017).

3. *Irradiance variation:* Temporal variation in irradiance causes PV modules to produce less power compared to a constant irradiance. The variation can occur through different environmental factors such as clouds, tree shades and dust etc.

3.1 Question 3.1

The $area_{available}$ is a fraction of the total available area on rooftops or facades (see equation 1a). For this report, the $area_{available}$ for the residential roof is 60% of the total area whereas for the office buildings, facades can be covered up to 30% of the total area and roofs can be covered up to 50% of the total area (equation 1a). To find the number of panels that can be mounted on the surfaces, the $area_{available}$ for PV installations is divided by the $area_{module}$ to calculate the number of panels that fit on the respective surfaces (equation 1b) . This calculation allows the subsequent calculation of the total capacity for a given surface by multiplying it with the capacity per module (equation 1c).

$$area_{available} = area_{surface} \cdot coverage_{surface} \tag{1a}$$

$$number\ of\ panels = \lfloor \frac{area_{available}}{area_{module}} \rfloor \tag{1b}$$

$$capacity_{surface} = number\ of\ panels \cdot capacity_{module} \tag{1c}$$

3.2 Question 3.2

To model the DC performance, the parameters, discussed in the beginning of this section (e.g., effective irradiance and module characteristics) need to be considered. The effective irradiance is determined using the DIRINDEX model, which uses irradiance, absolute air mass, angle of incidence, and the module characteristics as input parameters.

Also, module characteristics such as the cell temperature are dependent on the module construction and mounting technique. The mounting of PV panels is dependent on the surface characteristics. The flat roofs (Building A & B) are fitted with open-rack mounted PV panels, whereas pitched rooftops (Building C & D) and facades are mounted with close roof panels. To find the cell temperature of a module, the parameters defined in table 3 are used. Cell

temperature is an essential parameter to determine the performance of a cell. The results of the DC performance calculations, using cell temperature, are discussed in section 3.3 and 3.4.

Table 3: Cell temperature parameters for each cell type

Module	Mounting	a	b	ΔT[C]
c-Si/Cd Te	open rack	-3.47	-0.0594	3
c-Si/Cd Te	close roof	-3,7566	-0,156	2,58
HIT	open rack	-3,7489	-0.075	2,03
HIT	insulated	-2.81	-0.0455	0

3.3 Question 3.3

The annual DC yield is calculated by multiplying the sum of the DC performance of a panel by the number of panels on that surface (see question 3.2).
Figure 7 shows that the rooftop of building A has the highest annual yield of all surfaces for all PV panel types. In general, all surfaces of building A outperform the surfaces on other buildings. This is mainly due to the comparatively larger size of building A (see Table 4).

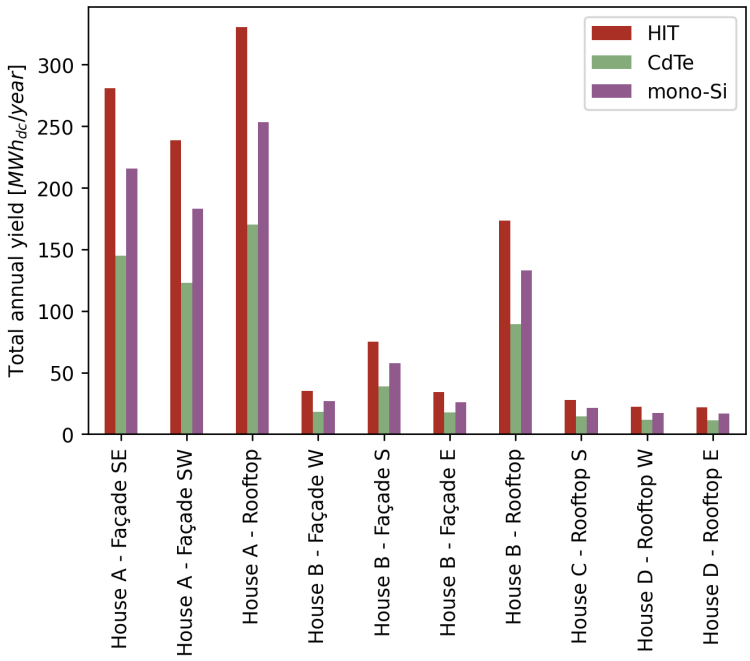

Figure 7: Total annual yield$_{DC}$ per module type and surface

3.4 Question 3.4

The plots in figure 7 and 8 show that HIT modules have the highest yield for all surface types across all buildings. The bar-chart in figure 8 replicate the same result. This renders HIT the "best" technology for all the building surfaces in producing high energy per unit area. Table 4 summarizes the best module type, number of modules installed on each surface, and the resulting total calculated capacity per surface.

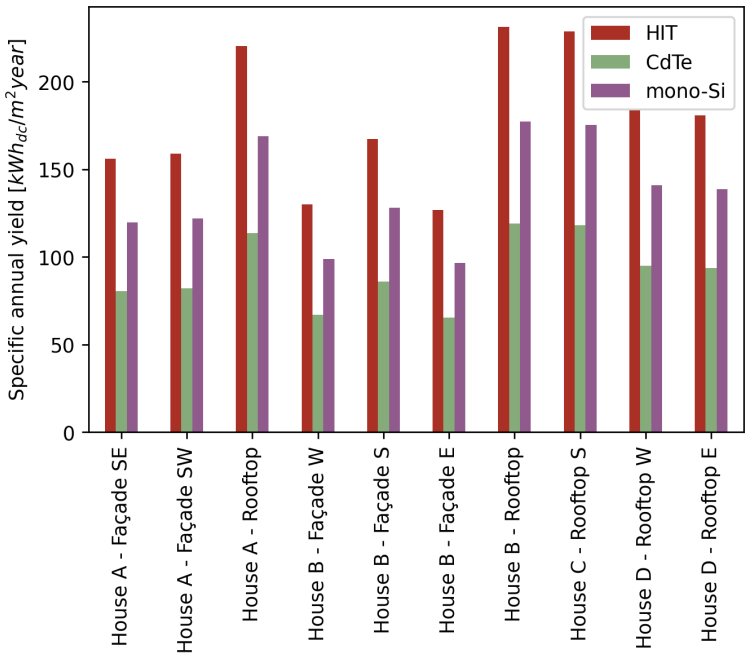

Figure 8: Specific annual yield$_{DC}$ for each surface

Table 4: PV characteristics per building and facade

Building	Building A			Building B				Building C	Building D	
Surface	Facade SE	Facade SW	Roof	Facade E	Facade S	Facade W	Roof	Rooftop S	Rooftop E	Rooftop W
Area [m^2]	6000	5000	3000	900	1500	900	1500	201.31	201.31	201.31
Coverage	30%	30%	50%	30%	30%	30%	50%	60%	60%	60%
Tilt [degrees]	90	90		90	90	90	35	40	40	40
Azimuth [degrees]	135	225	225	90	180	270	180	180	90	270
Module type	HIT	HIT	HIT	HIT	HIT	HIT	HIT	HIT	HIT	HIT
Number of modules	1428	1190	1190	214	357	214	595	95	95	95
Installed capacity [kW]	342.7	285.6	285.6	51.36	85.68	51.36	142.8	22.8	22.8	22.8

4 Calculating the AC power output

In section 4.1 and 4.2 the performance of the inverter and the AC output are determined. Section 4.3 presents an analysis of the performance of the panels throughout the year.

4.1 Question 4.1

The output of the solar panels is a direct current (DC), which will have to be converted to alternating current (AC) to be useful for most electrical applications.

To calculate the AC power output for each of the considered surfaces, a simplified mathematical inverter model is used, based on NREL's PVWatts model. This is done by calculating the efficiency of the inverter which is then multiplied by the DC output, as detailed by equations 2a to 2c. The efficiency is only used when the the DC power is larger than zero and smaller than the nominal DC power of the inverter, as specified by the conditions in equation 3.

$$P_{dc0} = \frac{P_{ac0}}{\eta_{nom}} \tag{2a}$$

$$\zeta = \frac{P_{dc}}{P_{dc0}} \tag{2b}$$

$$\eta = -0.0162 \cdot \zeta - \frac{0.0059}{\zeta} + 0.9858 \tag{2c}$$

$$P_{ac} = \begin{cases} \eta(P_{dc}) & : 0 < P_{dc} < P_{dc0} \\ P_{ac0} & : P_{dc} \geq P_{dc0} \\ 0 & : P_{dc} = 0 \end{cases} \tag{3}$$

4.2 Question 4.2

In figure 9 the total annual AC power production per facade is plotted for installations with HIT panels, as those were found to be the most effective. It clearly shows that building A produces the most power. This is confirmed in figure 10, which plots the total annual AC power output per building.

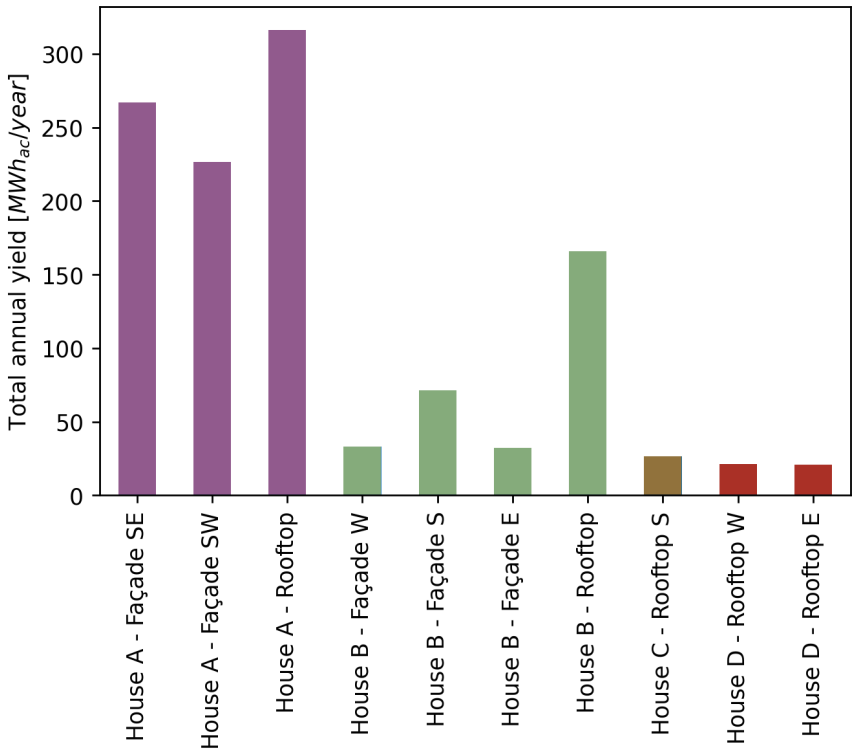

Figure 9: Total annual yield$_{AC}$ per surface

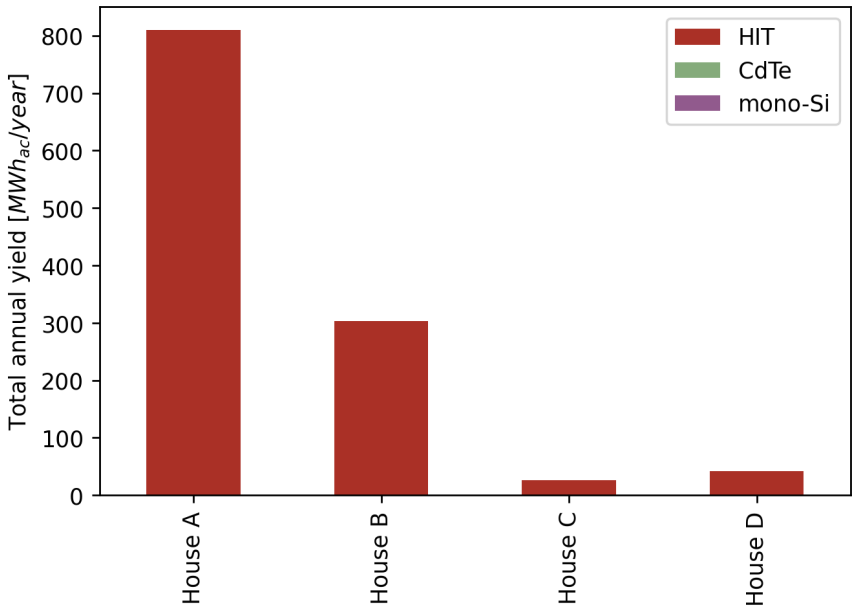

Figure 10: Total annual yield$_{AC}$ per building

4.3 Question 4.3

In figure 11 to 14 the hourly average power output of each buildings separate facades is shown for the dates April 21st, June 29th, and October 2nd 2019. The dates were chosen based on the instructions for this part of the exercise. It states that selected days should satisfy the

conditions of *(i)* representing days of higher irradiance during spring, summer and autumn and *(ii)* being sufficiently far apart from one another (*i.e.* not from the end of one month, followed by a day close to the beginning of the next month). The analysis of these figures can be found in question 4.4.

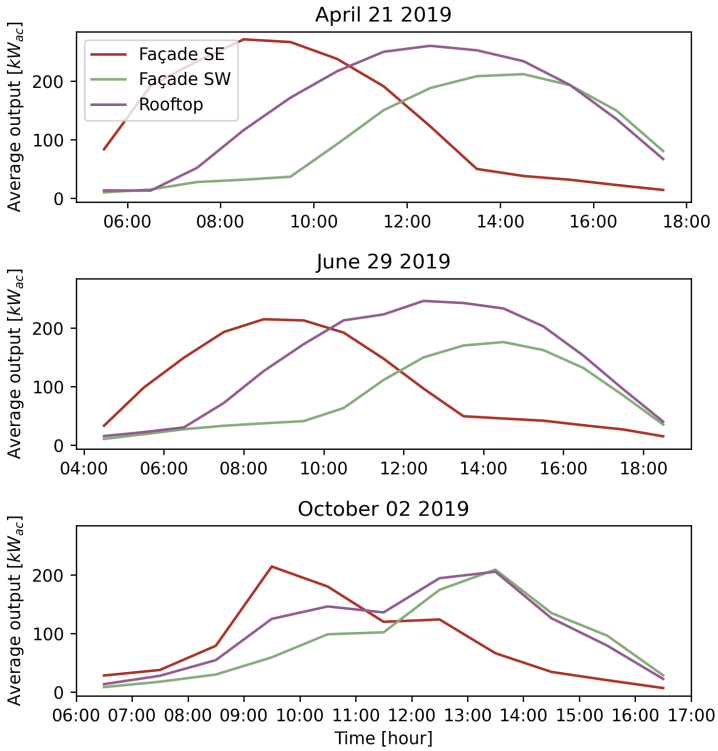

Figure 11: Power output of building A on April 21st, June 29th, and October 2nd 2019

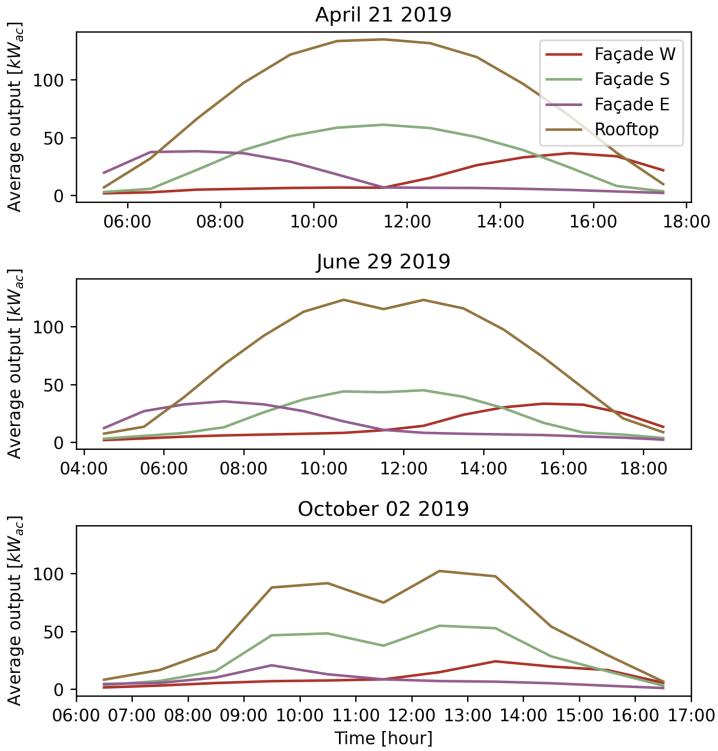

Figure 12: Power output of building B on April 21st, June 29th, and October 2nd 2019

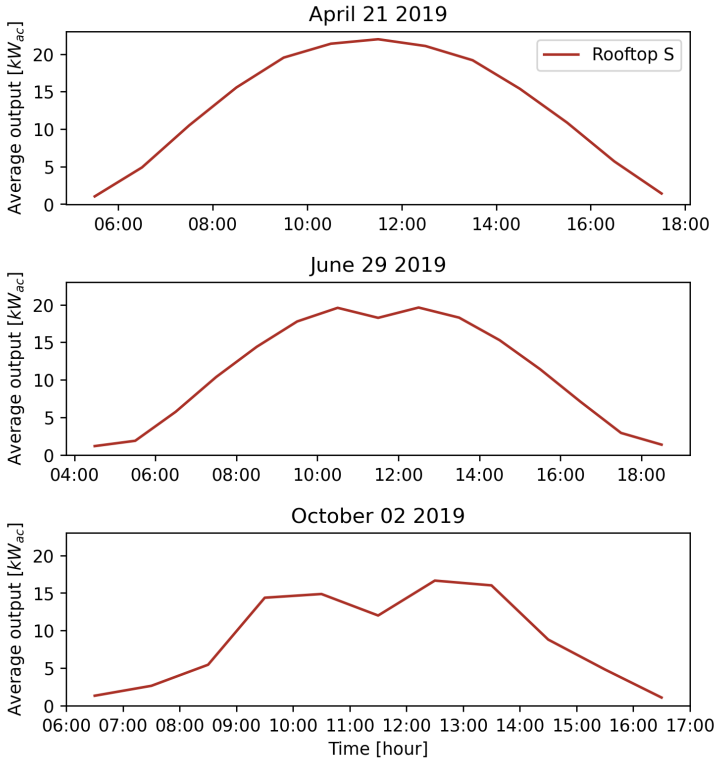

Figure 13: Power output of building C on April 21st, June 29th, and October 2nd 2019

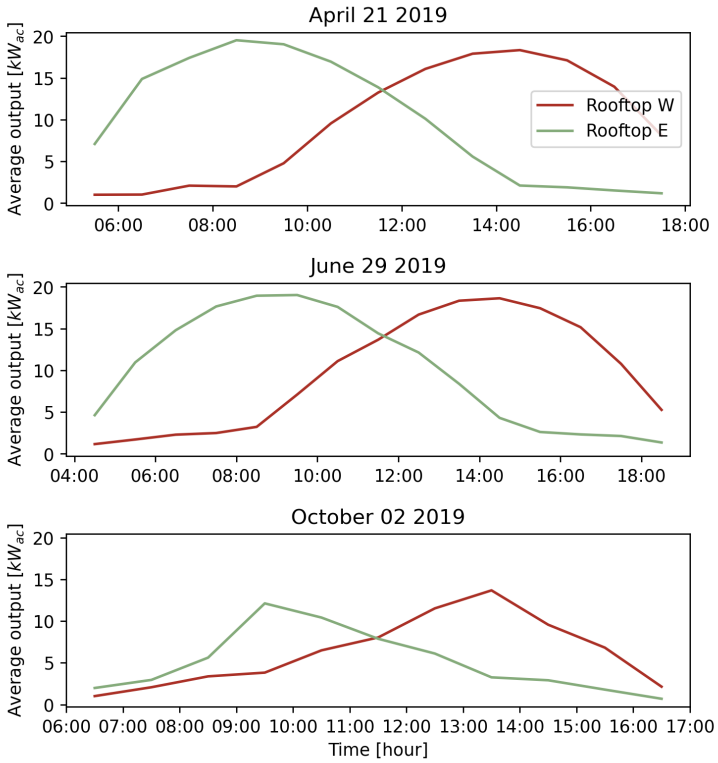

Figure 14: Power output of building D on April 21st, June 29th, and October 2nd 2019

4.4 Question 4.4

Figures 11 to 14 show three clear trends. The panels facing east have a production peak in the morning, panels facing south have a peak around mid-day, and panels facing west have a peak in the afternoon. These trends are expected since the sun is closest to a normal angle at those times of day for those respective positions.

There are also two trends on an annual scale. In spring and summer (April 21$^{\text{st}}$ and June 29$^{\text{th}}$) power production is noticeably higher than in autumn (October 2$^{\text{nd}}$) across all buildings and surfaces. The second annual trend visible is the change in daylight hours throughout the seasons, which determine the productive hours of the PV system. While in April and June the PV systems appear to produce a power output for roughly 13 hours a day, the productive time drops significantly during autumn season to roughly 10 hours a day. The figures also show that electricity generation starts much earlier in spring and summer (around 6am and 4:30am respectively) than during autumn season (around 7am), while ending one hour earlier as well (5pm in autumn as opposed to 6pm in Spring and Summer). This effect might be explained in part by the daylight savings hour time convention of the earlier seasons.

The third noticeable difference between the seasons is that the ramp up and ramp down times of power production before and after daily peaks is much shorter in autumn as compared to spring and summer. This is likely due to the shortened daylight hours and the fact that the sun rises to its zenith and falls to the horizon much quicker during autumn.

References

KNMI. (2019). Uurwaarden van weerstations. https://www.daggegevens.knmi.nl/klimatologie/uurgegevens.

Kunaifi, K., Reinders, A., Lindig, S., Jaeger, M., & Moser, D. (2020). Operational performance and degradation of pv systems consisting of six technologies in three climates. *Applied Sciences*, *10*(16), 5412.

Vidyanandan, K. (2017). An overview of factors affecting the performance of solar pv systems. *Energy Scan*, *27*(28), 216.

Wada, S. (2011). *A dictionary of color combinations*. Kyoto, Japan: Seigensha Art Publishing.